Journal of Environmental Chemical Engineering 9 (2021) 106725

Contents lists available at ScienceDirect

Journal of Environmental Chemical Engineering

journal homepage: www.elsevier.com/locate/jece

Sorption enhanced ethanol steam reforming on a bifunctional Ni/CaO catalyst for H_2 production

Maria Cortazar [a], Shuzhuang Sun [b], Chunfei Wu [b], Laura Santamaria [a], Leire Olazar [a], Enara Fernandez [a], Maite Artetxe [a], Gartzen Lopez [a,c], Martin Olazar [a]

[a] Department of Chemical Engineering, University of the Basque Country UPV/EHU, P.O. Box 644, E48080 Bilbao, Spain
[b] School of Chemistry and Chemical Engineering, Queen's University Belfast, Belfast BT7 1NN, UK
[c] IKERBASQUE, Basque Foundation for Science, Bilbao, Spain

ARTICLE INFO

Editor: V. Victor

Keywords:
Steam reforming
Ethanol
CO_2 capture
Hydrogen
Ni/CaO

ABSTRACT

The activity and stability of a 10 wt%NiO/CaO catalyst were tested in the sorption enhanced ethanol steam reforming (SEESR) in a fluidized bed reactor. The effect of temperature in the 600–750 °C range was analyzed and the performance of the catalyst at 700 °C was assessed by conducting cycles of SEESR reaction and CO_2 desorption. At zero time on stream, an increase in temperature enhanced ethanol steam reforming reactions, and therefore H_2 production increased from a yield of 20.3 wt% at 600 °C to 22 wt% at 750 °C. However, high temperatures hindered the catalyst sorption performance, i.e., CO_2 capture declined from 7.9 to 2.1 $mmol_{CO2}$ g_{cat}^{-1}. In order to evaluate the catalyst performance throughout the cycles and relate it with its features, both fresh and deactivated catalysts were characterized in detail by N_2 adsorption-desorption, X-ray fluorescence (XRF), X-ray diffraction (XRD), temperature programmed reduction (TPR) and oxidation (TPO) and transmission electron microscopy (TEM). Subsequent to 12 cycles, the catalyst CO_2 capture performance was slightly lower than that of the fresh one (approximately 7%) and hardly changed in the next cycles. Furthermore, the use of the same temperature for SEESR reaction and CO_2 desorption led to the highest adsorption capacity of the catalyst over multiple cycles.

1. Introduction

Humans are increasingly contributing to climate change and global mean temperature rise by over-exploitation of fossil fuels, cutting down forests and livestock farming. Thus, great amounts of greenhouse gases are added to those naturally present in the atmosphere, accelerating the greenhouse effect and global warming. EU's 2030 climate target plan proposes to reduce greenhouse gas emissions from energy, industry and transport sectors by at least 55% by 2023 and become climate neutral by 2050 [1–3].

Hydrogen makes viable the decarbonisation of industrial processes by reducing carbon emissions, as it only produces water after combustion. Up to present, hydrogen represents a modest fraction of the worldwide energy mix and is almost fully produced from non-renewable resources, such as natural gas or coal. Therefore, the development of hydrogen production technologies from renewable energy sources, such as biomass or biomass-derived feedstock, has been considered as a vital strategy to achieve the European Green Deal [4–7].

Among the diverse bio-based products, ethanol has generated a growing interest in recent years due to its high hydrogen content, wide availability, low cost, non-toxicity, easy handling and storage, and safety matters. Ethanol catalytic steam reforming is considered as the route with the highest potential to produce hydrogen. However, this process is a rather complicate one involving a wide variety of reactions, which lead to several undesired by-products. Moreover, the reversible nature of these reactions results in low H_2 yields, with the maximum theoretical H_2 purity being as low as 75%. Since the reaction pathway is very complex, H_2 yield and selectivity are strongly influenced by reaction conditions (temperature, S/C ratio and space-time) and catalyst formulation [8–11]. Thus, efforts have been directed towards the development of active and selective catalysts to enhance H_2 production. Although noble metal catalyst, such as Pt, Ru, Re, Rh and Pd, showed high activity and stability for ethanol steam reforming, they are so expensive that are industrially unviable [12–14]. Ni-based catalysts are highly active for C-C bond breakdown, which makes them a suitable choice for steam reforming processes. However, they are prone to coke

E-mail address: gartzen.lopez@ehu.eus (G. Lopez).

https://doi.org/10.1016/j.jece.2021.106725
Received 26 July 2021; Received in revised form 29 October 2021; Accepted 31 October 2021
Available online 5 November 2021

formation, and therefore undergo fast deactivation [15–17].

Many different supports have been used to make Ni based catalysts, with γ-alumina being the most used one [18–24]. Recently, CaO supports have attracted great attention, as they can capture CO_2 [25–31]. These catalysts are known as bifunctional catalysts and combine catalytic and sorption properties in one material, possessing exceptional advantages over their monofunctional counterparts [32,33]. This hybrid process of CO_2 capture and catalytic reforming of ethanol is called sorption-enhanced steam reforming, and is based on Le Chatelier's principle. Thus, bifunctional catalysts contribute to shifting the reaction equilibrium towards H_2 production by the in-situ removal of CO_2 [34–36]. According to this strategy, operation temperature may be lowered, and catalyst deactivation by sintering or coking may therefore be reduced [37,38].

CaO-based solids are considered efficient sorbents for CO_2 capture due to their thermal stability, high theoretical CO_2 sorption capacity (0.786 g_{CO2} g_{CaO}^{-1}), broad availability, low cost, and fast carbonatation/calcination kinetics. During the operation, CaO undergoes sorption/desorption cycles based on the reversible gas-solid carbonatation reaction involving CaO with the CO_2 in the product stream, forming $CaCO_3$ in the capture stage [39–41].

CaO carbonatation is an exothermic reaction consisting of an initial fast reaction step followed by a substantially slower second reaction step. In the first step, CO_2 is rapidly chemisorbed on the CaO surface, generating a thick layer of $CaCO_3$ around the CaO, whereas, in the second step, CO_2 is slowly diffused through the thick layer of $CaCO_3$, reacting with the inner unreacted CaO [42,43]. However, this process faces two main challenges: (i) sorption capacity loss over successive carbonatation/calcination cycles due to the high temperatures used in the desorption step, which leads to CaO sintering (ii) loss of the physical strength of the sorbent material, which leads to its attrition [44–46].

This paper assesses the potential benefits of using a bifunctional 10 wt%NiO/CaO catalyst in the sorption enhanced ethanol steam reforming (SEESR) in a micro-fluidized bed. The effect of temperature on the in-situ CO_2 capture and H_2 production was investigated in the 600–750 °C range and 700 °C was selected as the optimum temperature to analyse the stability of the catalyst in the cyclic operation. The novelty of this paper is associated with catalyst regeneration. Thus, operation with the same temperature in the SEESR reaction and CO_2 desorption is proposed to improve the catalyst stability over multiple cycles. Moreover, a thorough characterization (BET surface area, X-ray fluorescence (XRF), X-ray diffraction (XRD), temperature programmed reduction (TPR) and oxidation (TPO), and transmission electron microscopy (TEM)) of the fresh and spent catalysts was conducted to determine the main cause of the decay in activity and CO_2 capture capacity.

2. Experimental

2.1. Catalyst synthesis

The Ni/CaO catalyst was prepared by wet impregnation. Ni loading was determined by accurately controlling the ratio of CaO to Ni^{2+} chemicals (10 wt%NiO/CaO). After mixing all the chemicals together and stirring at room temperature for 1 h, temperature was raised to 85 °C to evaporate the excess water. It was then dried overnight in an oven at 130 °C and calcined in a muffle furnace at 750 °C for 5 h. The heating rate in the calcination step was 2 °C min^{-1}. Moreover, a commercial Ni catalyst (G90LDP) provided by SüdChemie was used for comparison purposes. This catalyst has a NiO content of 14 wt%, and is supported on Al_2O_3 and doped with Ca. Its characterization can be found elsewhere [47]. In addition, the catalysts were ground and sieved to a particle size between 250 and 400 μm, as this size was determined to be suitable for using in this micro-fluidized bed reactor. Before testing the catalysts, they were fluidized in a methacrylate spouted bed contactor for several hours in order to round the particles, improving their mechanical strength and therefore, minimizing possible attrition problems.

2.2. Characterization techniques

The physical properties of the catalyst (specific surface area, pore volume and average pore size) were determined by Micromeritics ASAP 2010 automatic adsorption equipment. BET and BJH methods were applied to the N_2 adsorption–desorption isotherms at 77 K.

X-ray diffraction (XRD) was conducted to identify the crystalline structure of the fresh and deactivated catalysts by using a *Bruker D8 Advance diffractometer* with CuKα radiation at 1.5406 Å wavelength. Data were continuously registered from 10° to 90° 2θ range. The diffraction spectra were indexed by their comparison with JCPDS files (Joint Committee on Powder Diffraction Standards). The crystallyte size of the phases were obtained from Scherrer equation using the full width at half maximum (FWHM) of the most intense line in each phase.

X-ray fluorescence (XRF) spectrometry was used to measure the chemical composition (wt%) of both fresh and deactivated catalysts. The chemical analysis of the particles was carried out under vacuum atmosphere using a sequential wavelength dispersion X-ray fluorescence (WDXRF) spectrometer (Axios 2005, PANalytical) equipped with a Rh tube, and three detectors (gaseous flow, scintillation and Xe sealing). The calibration lines were determined by means of well-characterized international patterns of rocks and minerals.

Temperature programmed reduction (TPR) was performed to determine the reducibility of the catalyst in an AutoChem II 2920 Micromeritics. Around 200 mg of fresh catalyst were placed in a U-shape tube, which was heated to 900 °C at a rate of 10 °C min^{-1} in a reducing atmosphere (10 vol% hydrogen in argon). A thermal conductivity detector (TCD) was used to analyze the hydrogen consumption of the samples, with its signal being recorded continuously.

Carbon deposition on the deactivated catalyst was monitored by temperature-programmed oxidation (TPO) in a Thermobalance (TGA Q5000 TA Instruments). Around 20 mg of deactivated catalyst were placed in a plate and heated under N_2 atmosphere to 500 °C to decompose $Ca(OH)_2$. The sample was then cooled down up to 200 °C and N_2 was changed for air and heated to 800 °C at a ramp of 5 °C min^{-1}. It was then hold for 30 min to ensure total carbon combustion.

The nature of coke was analyzed by *Philips CM200* transmission electron microscopy (TEM). Nanometer level catalyst images were obtained with a supertwin lens (0.235 nm point resolution), equipped with a 137.4 eV resolution EDX (energy dispersive X-ray spectroscopy) microanalysis system. The samples were placed in a double inclination sample holder (Philips PW6595/05) under vacuum to obtain the images.

2.3. Experimental equipment

Ethanol steam reforming experiments were carried out in the micro-fluidized bed reactor shown in Fig. 1. The main element of the experimental setup is the Inconel reactor, which is 10 mm in internal diameter and 300 mm long. The reactor is placed within a radiant oven and temperature was controlled by two thermocouples: one placed in the catalyst bed and other one close to the wall of the electric oven. Thus, solid circulation ensures temperature homogeneity in the whole reactor. Nitrogen was fed during the heating process and its flow rate was measured by a mass flow meter (Brooks SLA5800), which allowed feeding up to 1 L min^{-1}. Furthermore, the water flow rate was measured by a high pressure ASI 521 pump and that of ethanol by a syringe pump (Harvard apparatus PHD 4400). Both ethanol and water were vaporized and mixed within an evaporator located below the fluidized bed reactor. As the catalyst bed was placed in the middle section of the reactor supported on a very fine stainless steel mesh (<90 μm), the reactant gases had enough time to be preheated before contacting the bed. Moreover, another fine mess was placed at the reactor outlet in order to avoid catalyst entrainment during the experiments. The volatile stream leaving the reactor passed through a stainless steel filter (60 μm) and coalescence filter to ensure total condensation of the liquid products prior to collecting the permanent gases in a Tedlar bag.

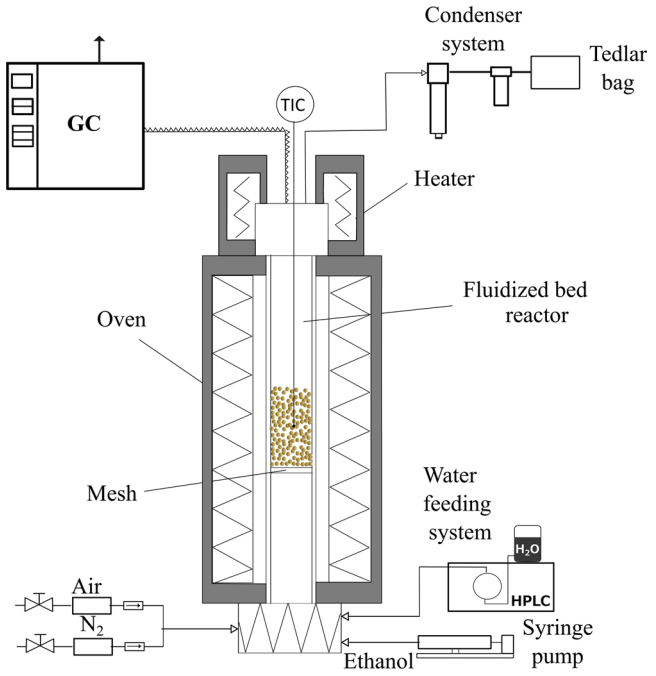

Fig. 1. Schematic diagram of the experimental system.

2.4. Operating conditions

Steam reforming experiments were performed in the 600–750 °C temperature range using steam as fluidizing gas. Thus, a water flow rate of 0.24 mL min^{-1} was employed and ethanol (96 vol%; 0.8905 kg L^{-1} density) was fed at a rate of 0.0725 mL min^{-1}, which corresponds to a steam/ethanol (S/E) ratio of 3.3 (S/C=4.8). The bed consisted of 1.5 g of Ni/CaO catalyst, with particle size being in the 250–400 μm range, which accounted for a space-time of 20 g_{cat} min mL_{EtOH}^{-1}. It should be also noted that the comparative experiments of conventional steam reforming on a Ni/Al_2O_3 commercial catalyst were performed under the same experimental conditions (temperatures, S/C ratio and space time). Prior to the reactions, the catalyst was subjected to an ex-situ reduction process at 710 °C for 4 h with a stream containing 10 vol% of H_2, being the total flow rate 100 mL min^{-1} (10 mL min^{-1} H_2 + 90 mL min^{-1} N_2).

Each reaction lasted 8 min, which is the time corresponding to catalyst saturation, as longer times led to a decrease in its capacity for CO_2 capture. All the gases produced during this time were collected into a Tedlar bag. After catalyst saturation, the feeds of ethanol and steam were cut off and the flow was switched to 300 mL min^{-1} of N_2 to regenerate the catalyst. CO_2 desorption was carried out using the same temperature as in the ethanol steam reforming runs.

Among all the temperatures tested, 700 °C was chosen to evaluate the catalyst performance by cycles, as it strikes a balance between the time needed for CO_2 desorption and the joint process of in-situ CO_2 capture and H_2 production. Overall, 22 cycles of SEESR and CO_2 desorption were performed. The experimental procedure followed was the same as for the runs at zero time on stream. Thus, the gases generated during the first 8-minutes SEESR reaction were collected in a Tedlar bag. Subsequently, ethanol and steam feeds were stopped and 300 mL min^{-1} of N_2 was introduced to desorb the CO_2. The temperature was maintained at 700 °C in both reaction and desorption steps. This procedure was repeated 22 times, in which the spent catalyst was subjected to CO_2 desorption process in order to decompose $CaCO_3$.

The mass balance was closed based on the quantification of carbon in the product gas by means of micro-GC and GC techniques. The amount of adsorbed CO_2 was calculated in order to attain a balance closure above 95% for carbon, hydrogen and oxygen under all the experimental conditions.

2.5. Product analysis

Samples of the volatile stream were analysed on-line by means of a GC Agilent 7890 chromatograph provided with a flame ionization detector (FID). The sample was injected into the GC through a line thermostated at 280 °C to avoid the condensation of heavy compounds. However, the non-condensable gases were analyzed off-line in a micro GC (Varian 4900) equipped with three modules (molecular sieve, Porapak (PPQ) and plot alumina) and thermal conductivity detectors (TCD). The micro-GC was also used to monitor the CO_2 desorption process, but in this case, it was used on-line.

2.6. Reaction indices

Several reaction indices were defined in order to assess the performance of Ni/CaO catalyst in the SEESR process. The yield of each gaseous compound was defined by mass unit of the ethanol fed into the reactor, which is calculated as follows (Eq.(1)):

$$Y_i = \frac{m_i}{m_{EtOH}} \cdot 100 \quad (1)$$

where m_i and m_{EtOH} are the mass flow rates of each compound and the ethanol feed into the reactor, respectively. Note that these yields are not the result of a carbon balance to the compounds.

The maximum theoretical H_2 yield was determined as a percentage of the maximum allowed by stoichiometry (Eq.(2)).

$$Y^0_{H_2} = \frac{m_{H_2}}{m^0_{H_2}} \cdot 100 \quad (2)$$

where m_{H2} is the H_2 mass flow rate and m^0_{H2} the maximum allowable by stoichiometry.

CO_2 adsorption efficiency (Eqn 3) was expressed as the amount of CO_2 captured during the reaction divided by the total amount of CO_2 produced in the ethanol steam reforming, which is the sum of the CO_2 adsorbed by the Ni/CaO catalyst and the average CO_2 produced in the sorption enhanced ethanol steam reforming during the first 8-minute reaction.

$$CO_2 \text{ adsorption } \textit{efficiency}, \quad \%: \frac{m_{CO_2 ads}}{m_{CO_2 total}} \cdot 100 \quad (3)$$

3. Results

3.1. Catalyst characterization

Table 1 shows the physical properties and chemical composition of

Table 1
Physical properties and chemical composition of the fresh Ni/CaO catalyst.

	Ni/CaO
Physical properties	
S_{BET} (m^2 g^{-1})	3.16
V_{pore} (cm^3 g^{-1})	0.012
d_{pore} (Å)	237.3
*Average crystallite size (nm)**	
Ni	58
Chemical composition (wt%)	
MgO	0.70
SiO_2	0.30
NiO	9.66
CaO	82.33
Al_2O_3	0.52
TiO_2	0.03
P_2O_5	0.05
Fe_2O_3	0.06

* Calculated at 2Θ= 44° for Ni from X-ray diffraction patterns.

the fresh 10 wt%NiO/CaO catalyst. Thus, surface area and pore volume are essential parameters in CO_2 adsorption processes. The surface area of the catalyst gives an indication of the area available for CO_2 adsorption and the pore volume determines the space for CO_2 diffusion through the adsorbent [48]. As observed, the specific surface area of the catalyst was rather low (3.16 m^2 g^{-1}) and the pore volume of 0.012 cm^3 g^{-1} was evidence of a non-developed porous structure. Moreover, the results also show that it was a slightly mesoporous material because its pore size was in the 2–50 nm range. Sang et al. [49] reported similar physical properties for the Ni/CaO catalyst. However, other authors synthesized a Ni/CaO catalyst with a higher surface area (around 15 m^2 g^{-1}), with CaO being prepared by the sol-gel method [28,50,51]. In fact, the catalyst synthesis method can affect the morphology and properties of CaO [52–55].

The NiO content of the catalyst determined by XRF analysis was 9.66 wt%, which is very consistent with the intended metal loading of 10 wt%. The crystallite size of the Ni metal was calculated based on the Scherrer equation.

As shown in Fig. 2a, the XRD pattern of the reduced Ni/CaO catalyst revealed that it was composed of CaO, $Ca(OH)_2$, NiO and Ni^0. $CaCO_3$ was not observed, which is evidence that CaO carbonatation during storage did not occur. Undoubtedly, the most intense diffraction lines belonged to CaO located at 2Θ= 32, 38 and 55°. The intensity of the other diffraction lines was much lower than for CaO. The $Ca(OH)_2$ diffraction peaks indicated that CaO absorbed humidity from the atmosphere to form $Ca(OH)_2$ (CaO is a highly hygroscopic material). The presence of this compound was also observed by several authors [28,50,56]. However, before starting ethanol steam reforming reactions, this compound was eliminated from the catalyst, as reaction temperatures were higher than that required for $Ca(OH)_2$ decomposition in all the runs. The presence of NiO was evidence of its incomplete reduction to nickel metal. It seems that H_2 did not reach all the Ni sites in the catalyst, as NiO was possibly coated with CaO. Sang et al. [56] also observed both Ni and NiO in the 5 wt%Ni/CaO catalyst.

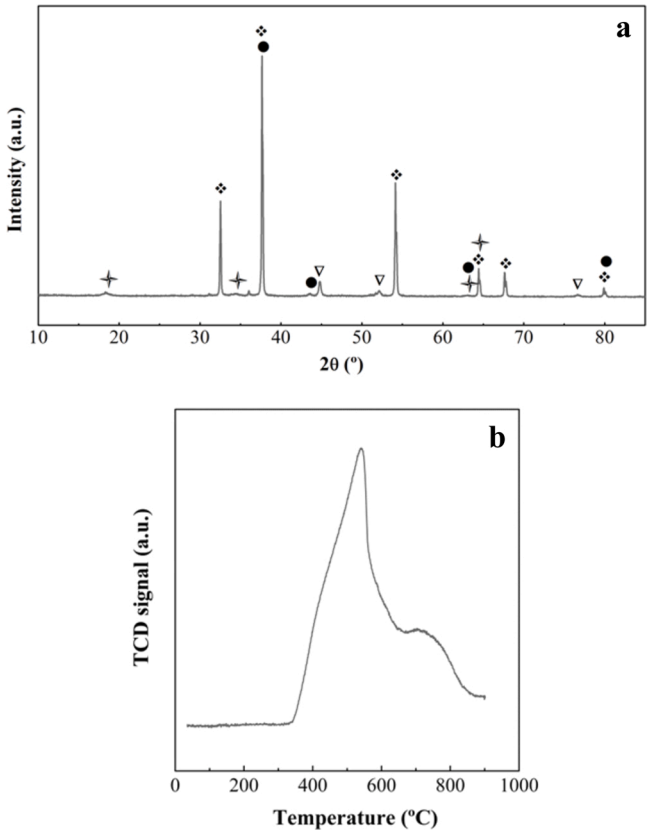

Fig. 2. X-ray diffraction (XRD) patterns (a) and TPR profile (b) of the reduced Ni/CaO catalyst. Crystalline phases: (+) $Ca(OH)_2$, (❖) CaO, (•) NiO and (▽) Ni^0.

The temperature programmed reduction (TPR) profile of the Ni/CaO catalyst is shown in Fig. 2b, and it enables determining the temperature needed for the reduction of metallic species. It is well-known that the profile depends not only on the nature of the metallic species, but also on the metal-support interactions. The reduction profile of 10 wt%NiO/CaO catalyst had two main peaks located at 500 °C and 720 °C. A third one may also be observed at a reduction temperature of 400 °C overlapped with the peak at 500 °C. The first two peaks were easily reducible species due to their low reduction temperature (400 and 500 °C). The former was due to the reduction of bulk NiO, with minimal or no interaction with the support, and the latter to the reduction of NiO located on the catalyst surface, which had a significant interaction with CaO. Given the great diversity of compounds shown in the XRF analysis, no clear associations may be established for the peak located at 720 °C. However, this peak may be attributed to the very strong interaction of Ni with some of the compounds detected by XRF, probably Al_2O_3 or MgO, as they are not easily reduced. No diffraction lines were observed in the XRD spectra for any Ni solution, which was probably because they overlapped with other diffraction lines or cannot be identified due to its poor crystallinity.

3.2. *Effect of temperature at zero time on stream*

The SEESR is an exothermic process defined by the following reaction (Eq.(4)):

$$C_2H_5OH + 3\,H_2O + 2\,CaO \rightarrow 6\,H_2 + 2\,CaCO_3\ \Delta H^\circ = -185.3\ kJ\ mol^{-1} \quad (4)$$

However, the reaction mechanism is complex due to parallel secondary reactions generating intermediate products and by-products. Side reactions, such as dehydrogenation (Eq.(5)), decomposition (Eq. (6)) and dehydration (Eq.(7)) of ethanol, steam reforming of methane and ethylene (Eqs, (8) and (9)) and WGS (Eq.(10)) take place in parallel with the main reaction. Thus, the efficiency of the process strongly depends on selecting adequate reaction conditions (temperature, S/E ratio and space time) and catalyst composition. The optimum temperature is the one striking a balance between thermodynamics and kinetics [57].

$$C_2H_5OH \rightarrow CH_3CHO + H_2 \quad (5)$$

$$C_2H_5OH \rightarrow CH_4 + CO + H_2 \quad (6)$$

$$C_2H_5OH \rightarrow C_2H_4 + H_2O \quad (7)$$

$$CH_4 + H_2O \leftrightarrow CO + 3H_2 \quad (8)$$

$$C_2H_4 + 2H_2O \rightarrow 2\,CO + 4H_2 \quad (9)$$

$$CO + H_2O \leftrightarrow CO_2 + H_2 \quad (10)$$

Temperature was varied in the 600–750 °C range and its influence on gas composition is shown in Fig. 3. As observed, an increase in temperature leads to a lower hydrogen content in the gaseous stream, as the overall SEESR reaction is thermodynamically hindered as temperature is increased due to its exothermic nature [58]. Thus, hydrogen concentration decreased from 85.95 vol% at 600 °C to 75.18 vol% at 750 °C. Furthermore, the concentration of CO increased by increasing temperature, reaching a value of 6.29 vol% at 750 °C, which is evidence that CO_2 adsorption decreased and a lower amount of CO underwent WGS reaction (Eq.(10)) due to the equilibrium displacement towards the reverse reaction. The concentration of methane also decreased as temperature was raised, since its steam reforming (Eq.(8)) was promoted [48]. It should be noted that CO_2 removal at high temperatures may efficiently hinder the methanation reaction, lowering CH_4 concentration in the gaseous product stream [57]. The concentration of the C_2-C_4

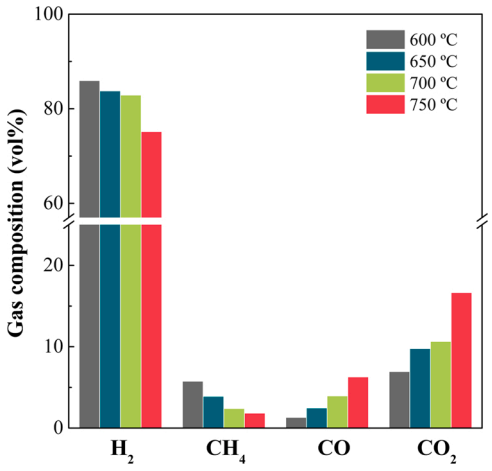

Fig. 3. Effect of temperature on the gas composition in the 600–750 °C temperature range (S/E=3.3; τ=20 g_{cat} min mL_{EtOH}^{-1}).

hydrocarbon fraction was negligible under the temperature range studied, which is evidence that, under these reaction conditions, steam reforming reactions involving light hydrocarbons (Eq.(9)) were enhanced. The previous results proof that operation at 600 °C with this bifunctional catalyst allowed capturing effectively the CO_2 generated in the SEESR process, leading to the shift of the thermodynamic equilibrium towards high purity hydrogen production [56]. It should be noted that the adsorption process involves the chemical reaction of CaO with CO_2 in the product stream in order to form $CaCO_3$.

Fig. 4 shows the effect temperature has on the yield of the products. It should noted that CO_2 yield was divided into two fractions; i) the CO_2 adsorbed on the Ni/CaO catalyst and ii) the CO_2 in the gaseous product stream. It is noteworthy that ethanol conversion on the 10 wt%NiO/CaO catalyst was full in the 600–750 °C temperature range, as no acetaldehyde, acetic acid or acetone were detected in the product stream. According to Montero et al. [59], the reactions involving formation/consumption of these compounds are very fast or do not occur under these experimental conditions.

H_2 yield increased slightly with temperature in the 600–750 °C range

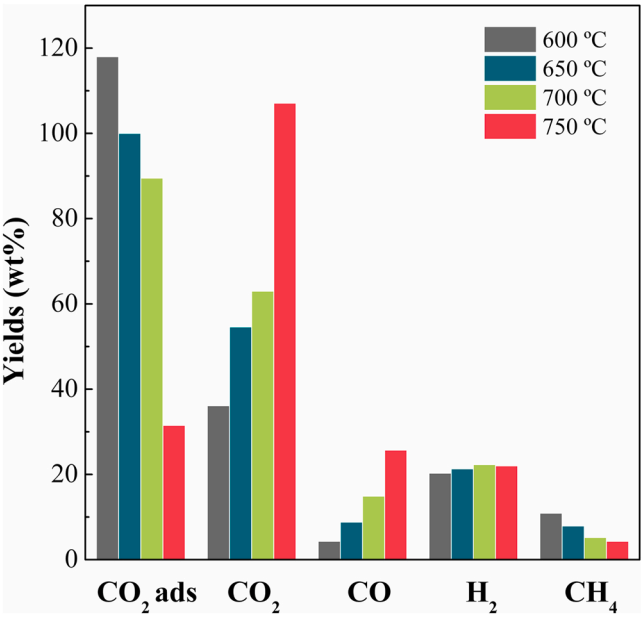

Fig. 4. Effect of temperature on the individual product yields in the 600–750 °C temperature range (S/E=3.3; τ=20 g_{cat} min mL_{EtOH}^{-1}).

from 20.3 to 22 wt%. In fact, it peaks at 700 °C (22.3 wt%). It seems that the decrease in CO_2 capture capacity was not fully balanced with the enhancement of ethanol steam reforming from 700 °C to 750 °C. Methane yield decreased from 10.9 wt% at 600 °C to 4.3 wt% at 750 °C and that of CO increases to 25.7 wt%, with the increase being more pronounced from 700 to 750 °C. These results are evidence that methane steam reforming reactions (Eq.(8)) were enhanced at high temperatures. When temperature was raised, the adsorption efficiency on the 10 wt% NiO/CaO catalyst decreased from 77% to 23%. Thus, in the 600–700 °C temperature range, the catalyst adsorption capacity decreased from 77% to 59%, while in the 700–750 °C range, it decreased from 59% to 23%. For temperatures above 700 °C, the amount of captured CO_2 decreased drastically, since CO_2 carbonatation rate was much lower due to the competition of CaO carbonatation and calcination reactions. From these results, it is clear that high temperatures inhibit CO_2 removal, yielding large amounts of CO_2 in the product stream (107.1 wt% at 750 °C).

The comparison of these results with those in the literature is a challenging task due to the diversity of the operating conditions used and adsorption capacities reported. Nevertheless, most of the authors [60–65] distinguish between pre-breakthrough and breakthrough stages, and followed the sorption performance of both sorbents and bifunctional catalysts in different processes.

A comparison of the conventional ethanol steam reforming with the sorption enhanced ethanol steam reforming showed that higher H_2 yields were obtained in the latter in the 600–750 °C temperature range (of around 20–22 wt%), even though full conversion was reached in both cases. Prior to the set of runs described in the experimental section, several tests with a commercial Ni/Al_2O_3 catalyst (14 wt% NiO) were carried out in this reactor to define the suitable operating conditions and confirm the effect of CO_2 adsorption. At 700 °C, similar H_2 productions (of around 22.2 wt%) were obtained with both catalysts, although the commercial catalyst had a higher metal loading, and therefore should have been more active in reforming reactions. However, more remarkable results were obtained concerning CO_2 production. Thus, Ni/Al_2O_3 catalyst produced 87.3 wt% of CO_2, whereas the NiO/CaO catalyst generated an average of 63.0 wt% of CO_2 after 8-min reaction. In the literature, Di Michele et al. [66] worked with 10 wt%$Ni/MgAl_2O_4$ catalyst in a downflow reactor and obtained 16.83 wt% H_2 at 625 °C. Olivares et al. [67] used 8 wt%Ni/CeO_2-$MgAl_2O_4$ and reported a higher H_2 yield of 19.56 wt% at 650 °C, which was explained by the improvement in catalyst dispersion when Ce is added. Furthermore, Bussi et al. [68] tested a Ni-La-Sn trimetallic catalyst in a fixed bed reactor at 650 °C and attained a lower H_2 yield of 16.56 wt%. However, Shao et al. [69] used a $LaNi_{0.85}Zn_{0.15}O$ perovskite structured catalyst at 700 °C without CO_2 capture and reported a H_2 yield value (21.74 wt%) close to that obtained in this work.

The structural features and the amount of CaO influence the adsorption capacity per catalyst mass unit, with the balance between these two factors determining the CO_2 adsorption performance of the catalyst [50]. Moreover, the different techniques used for measuring the CO_2 uptake make it difficult a comparison of the results. TGA analysis has been widely used to determine the sorption capacity of sorbents. However, the experimental conditions in TGA are very different from those in the reforming reaction environment. Table 2 shows the adsorption capacity of the 10 wt%NiO/CaO catalyst at various

Table 2
CO_2 capture on the 10 wt%NiO/CaO bifunctional catalyst in the 600–750 °C temperature range.

Temperature (°C)	Adsorption capacity ($mmol_{CO2}$ g_{cat}^{-1})
600	7.9
650	6.7
700	6.0
750	2.1

temperatures.

As temperature was increased, the catalyst sorption capacity was hindered, and therefore declined from 7.9 to 2.1 $mmol_{CO2}\ g_{cat}^{-1}$. In this work, the maximum sorption capacity was obtained at 600 °C. Similar CO_2 adsorption capacities have been reported for the Ni/CaO catalyst under comparable temperature ranges. Thus, Chanburanasiri et al. [49] reported that 12.5 wt%Ni/CaO catalyst had a CO_2 sorption capacity of 5.06 $mmol_{CO2}\ g_{cat}^{-1}$ at 500 °C, which is consistent with the value obtained in this work at 600 °C. Wang et al. [27] obtained a slightly higher sorption capacity (7.43 $mmol_{CO2}\ g_{cat}^{-1}$) at 700 °C for the 10 wt% Ni/CaO catalyst. Furthermore, Jo et al. [51] reported much higher adsorption capacities for the 10 wt%Ni/CaO catalyst at 600 and 700 °C, i.e., 15.49 $mmol_{CO2}\ g_{cat}^{-1}$ and 16.22 $mmol_{CO2}\ g_{cat}^{-1}$, respectively. However, this catalyst was synthesized by the sol-gel method and its specific surface area was almost six times higher (16.8 $m^2\ g^{-1}$) than that of the one used in this study, which contributes to improving its initial sorption capacity. In the case of other CaO-based catalysts, Di Giuliano et al. [70] obtained a slightly higher sorption capacity for the 3 wt% Ni/CaO-mayenite catalyst (8.20 $mmol_{CO2}\ g_{cat}^{-1}$) at 650 °C.

3.3. Catalyst performance in reaction cycles

The evolution of gas composition throughout 22 reaction cycles on the10 wt%NiO/CaO catalyst is shown in Fig. 5 in order to evaluate the stability of the catalyst. As observed, the concentration profiles of the products in the outlet stream underwent a small decay or increase (depending on the product) up to the 12th cycle, and they then remained stable throughout the remaining cycles, until the 22 cycles were completed. H_2 concentration declined from 82.89 vol% in the first cycle to 78.02 vol% in the 12th cycle, and therefore those of CO and CH_4 increased from 3.95 and 2.40 vol% to approximately 6.2 vol%, with this value being unchanged for subsequent cycles. In addition, C_2-C_4 concentration also increased slightly to 0.65 vol%. The change in gas composition over multiple cycles was due to the deterioration of catalyst sorption and reforming capacities. The decrease in sorption capacity shifted the equilibrium of WGS reaction (reverse WGS was enhanced), whereas the decay in catalyst reforming activity reduced the reforming extent of CH_4 and light hydrocarbons. At 700 °C, the reforming reactions involving CH_4 and C_2-C_4 hydrocarbons were much enhanced and they are not therefore affected by the WGS reaction.

The evolution of the products yields is plotted in Fig. 6. In order to ease the evaluation of process efficiency, this figure also shows the maximum theoretical H_2 yield defined based on the maximum allowable

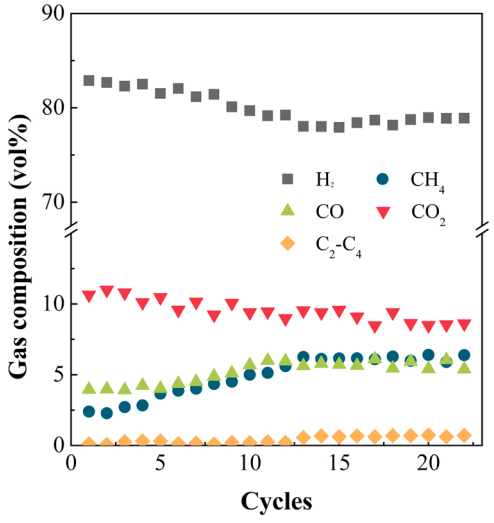

Fig. 5. Influence of CO_2 adsorption-desorption cycles on the gas composition. (T = 700 °C; S/E=3.3; τ =20 g_{cat} min mL_{EtOH}^{-1}).

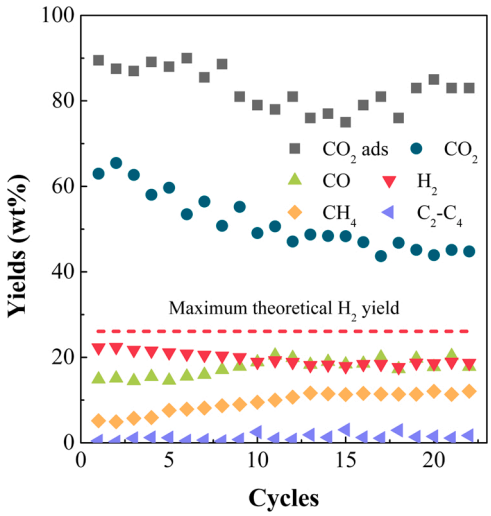

Fig. 6. Influence of CO_2 adsorption-desorption cycles on the product yields (T = 700 °C; S/E=3.3; τ =20 g_{cat} min mL_{EtOH}^{-1}).

by stoichiometry. Ethanol conversion was full during all the cycles, i.e., no ethanol was observed in the product stream. Moreover, intermediate products, such as acetaldehyde, were not observed. After 12 cycles the catalyst seemed to be relatively stable. Thus, it underwent a small decay in both CO_2 capture (7% lower) and reforming performance, and there was therefore a small variation in the products yields. H_2 production slightly declined from 22.24 wt% in the first cycle to 18.46 wt% in the 12th cycle and those of CO and CH_4 increased from 14.85 and 5.15 wt% to 17.64 and 11.96 wt%, respectively, with the increase in CH_4 being more pronounced. In turn, the C_2-C_4 yield also increased slightly to 1.71 wt%. The increase in CH_4 yield, and especially in that of C_2-C_4 hydrocarbons (they are very reactive), was evidence of the lower catalyst reforming activity. After multiple cycles, the extent of the steam reforming reactions involving CH_4 end C_2-C_4 hydrocarbons was lower than in the first cycle. Furthermore, as CO_2 capture capacity declined, a greater amount of CO_2 was in the reaction environment, and therefore the WGS reaction shifted to the left (reverse WGS was enhanced), thereby favouring CO production. In the case of H_2 yield, its decrease was due to the combined effect of both lower CO_2 capture and lower reforming extent on the bifunctional catalyst.

The adsorption capacity of the catalyst decreased from 6 to 5.6 $mmol_{CO2}\ g_{cat}^{-1}$ after 22 cycles, which accounts for 6.7% reduction. Thus, CO_2 capture capacity decreased during a few initial cycles, and it then stabilized, as was also reported by Aloisi et al. [71]. This result confirms that the use of the same temperature for desorption and ethanol steam reforming is beneficial for the catalyst stability. According to Wang et al. [27], this slight decrease in the carbonatation conversion over the initial cycles may be attributed to the agglomeration and sintering of CaO and carbon deposition on the surface of the catalyst.

More pronounced decays have been reported in literature for the same catalyst. Xu et al. [72] tested the stability of Ni/CaO catalyst at 650 °C during 10 cycles, and observed that CO_2 adsorption capacity decreased from 12.73 to 10.68 $mmol_{CO2}\ g_{cat}^{-1}$, which accounts for 16% reduction. Liu et al. [50] worked with the same catalyst and at the same temperature as the previous authors, but reported that the sorption capacity decreased by approximately 54% (from 10.23 to 4.77 $mmol_{CO2}\ g_{cat}^{-1}$) after 20 cycles. The same authors supported CaO on Al_2O_3 and concluded that Ni/CaO-Al_2O_3 catalyst stability was improved, since sorption capacity declined from 14.55 to 10.1 $mmol_{CO2}\ g_{cat}^{-1}$ after 20 cycles, which accounts for 31% reduction instead of 54% without Al_2O_3. Li et al. [73] followed the same strategy as the previous authors, but supported CaO on ZrO_2. The initial CO_2 capture capacity of

Ni/ZrO_2-CaO catalyst was lower (7.95 $mmol_{CO2}$ g_{cat}^{-1}) than that of Ni/CaO-Al_2O_3 catalyst, but this capture capacity remained over 15 cycles. $CaZrO_3$ may inhibit sintering during the carbonatation/calcination cycles.

3.4. Causes of bifunctional catalyst decay

Catalyst deactivation is the main factor conditioning viability and operation of any industrial catalytic process. Thus, the spent catalyst was characterized in detail in order to determine the main causes of catalyst activity decay.

In order to ascertain the deterioration of the porous structure, the deactivated catalyst was analyzed by N_2 adsorption-desorption. Table 3 shows the values of the specific surface area, pore volume and diameter for the reduced and deactivated Ni/CaO catalysts. After 22 cycles, the specific surface area of the catalyst, as well as the pore volume and their size, increased, which is attributed to the amount and morphology of the coke deposited and/or re-dispersion of CaO particles during the SEESR. Furthermore, the Ni crystallite size was also calculated at 2Θ= 44° for Ni from the X-ray diffraction pattern. The average Ni crystallite size increased from 58 to 155 nm, which is evidence that Ni sintered, and the dispersion of the bifunctional catalyst was therefore worse. Christensen et al. [74] reported that sintering is accelerated by large metal particles. Regarding CaO crystallites, it was estimated they decreased in size after 22 cycles, which is evidence of the structural changes undergone by the catalyst over the cycles. Although it seems that XRF analysis reveals small differences between the fresh and spent catalysts, it should be noted that the total amount of oxides was not the same in the fresh and deactivated catalysts. As shown in the XRD (Fig. 7a), the deactivated catalyst had a larger amount of $Ca(OH)_2$, which was obtained by decomposition during sample preparation before the XRF analysis.

The XRD pattern in Fig. 7a shows the changes in the metallic structure of the Ni/CaO catalyst after the cycles. The same species as in the fresh catalyst were found in the deactivated sample. The main crystalline structure was still CaO, although more diffraction lines of $Ca(OH)_2$ were identified in the deactivated catalyst as a result of introducing steam as fluidization agent. No significant changes in Ni^0 and NiO crystalline species were detected.

Coke deposition has been reported as the main catalyst deactivation cause in the reforming processes [75–79]. The intermediate reactions during ethanol steam reforming (dehydrogenation, dehydratation, polymerization and decomposition of different byproducts) are liable to form carbon deposits on the surface of the catalyst [16,80].

The morphology and nature of coke are determined by its combustion temperature. Thus, the combustion temperature of the coke

Table 3
Physical properties and chemical composition of the reduced and deactivated Ni/CaO catalyst.

	Ni/CaO *fresh/deact*
Physical properties	
S_{BET} (m^2 g^{-1})	4.26/6.40
V_{pore} (cm^3 g^{-1})	0.015/0.034
d_{pore} (Å)	232.3/291.5
*Average crystallite size (nm)**	
Ni	58/155
Chemical composition (wt%)	
MgO	0.70/0.67
SiO_2	0.30/0.50
NiO	9.66/9.06
CaO	82.33/71.92
Al_2O_3	0.52/0.66
TiO_2	0.03/0.03
P_2O_5	0.05/0.01
Fe_2O_3	0.06/0.09

* Calculated at 2Θ= 44° for Ni from X-ray diffraction patterns.

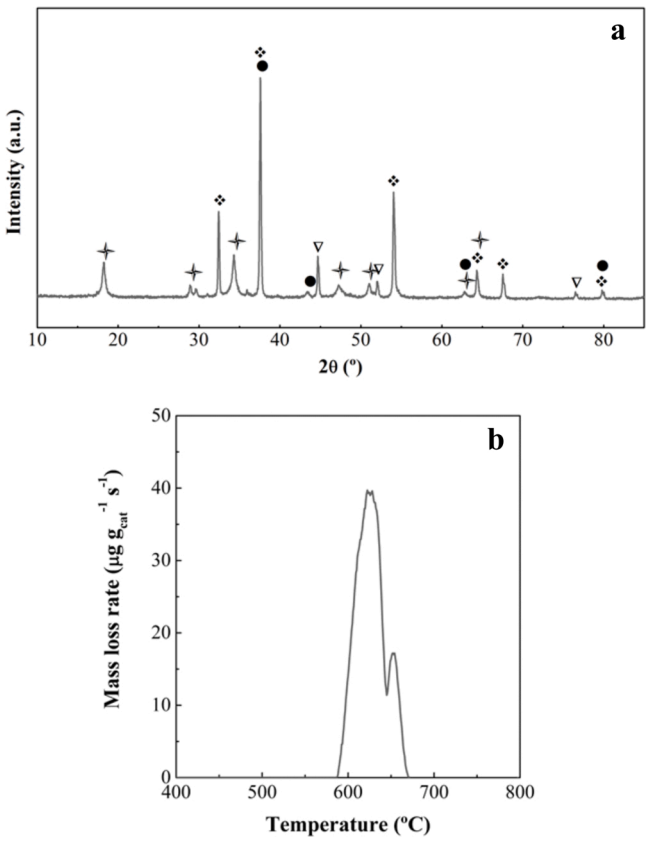

Fig. 7. XRD pattern (a) and TPO profile (b) of the deactivated Ni/CaO catalyst. Crystalline phases: (+) $Ca(OH)_2$, (❖) CaO, (•) NiO and (▽) Ni^0.

encapsulating the Ni sites is low (Ni may activate coke oxidation), and that of the coke deposited on the support is higher [81–84]. Moreover, the coke deposited on similar locations may also have different combustion temperatures due to their condensation degree i.e., the higher the burning temperature the higher the condensation degree; that is, more organized structures with lower H/C ratios. The TPO profile of the spent Ni/CaO catalyst is shown in Fig. 7b, in which two oxidation peaks appear at around 623 °C and 653 °C. Both peaks were related to the coke deposited on the support, although there were small differences in their condensation degree. As explained in the experimental procedure, the catalyst was subjected to CO_2 desorption after the last cycle, and therefore TPO analysis did not show any peak corresponding to $CaCO_3$.

The total amount of coke and its characteristics vary with the operating conditions, such as the nature of the reformed compound, the catalyst and the reaction conditions, especially temperature and S/B ratio, as carbon deposition is a consequence of a balance between its formation and removal [85]. Thus, the total amount of carbonaceous deposits on the spent catalyst was 0.31 wt%.

Aceves et al. [86] studied the SEESR process by using a mixture of Ni/Al_2O_3 catalyst with CaO, and reported no carbon formation, whereas higher amounts of coke (14 wt%) were reported in the conventional ethanol steam reforming process. Likewise, Montero et al. [87] studied the deactivation of Ni/La_2O_3-Al_2O_3 catalysts in the conventional ethanol steam reforming using similar operating conditions as in this work (T = 650 °C; S/E=3; τ =0.18 g_{cat} h g_{EtOH}^{-1}), and coke formation was of 10.8 wt%.

In this study, a few factors inhibiting coke formation were gathered. At 700 °C, WGS reaction led to an increase in hydrogen production, and therefore carbon deposition decreased. Moreover, more water than that corresponding to stoichiometry was used, which also had an inhibitory effect on coke formation. The catalyst support may also contribute to generating carbonaceous matter on the catalyst surface. Accordingly,

CaO was used as catalyst support and, since it is basic, intermediate hydrocarbon (ethylene and methane) deposition and Boudouard reaction were hindered, and therefore coke formation decreased. Additionally, calcium enables water dissociation for producing sufficient O intermediates for C oxidation [88].

The TEM images of the deactivated 10 wt%NiO/CaO catalyst are presented in Fig. 8, in which the location and morphology of the deposited coke may be observed. In these images, Ni^0 particles are identified as dark areas, whereas the grey shapes are related to CaO support. Moreover, an incipient formation of the coke deposited (blurred filaments) is also observed, which has a structured morphology. It seems that all the coke was mainly deposited on the support, which was also deduced from the TPO analysis. This structured and filamentous coke did not block Ni particles, even though its progressive deposition may hinder the contact between reactants and Ni particles. In addition, a tip-growth mechanism may be responsible for the filamentous carbon formation, as Ni particles were above the coke. In the case of large metal particles, carbon deposits had a weak binding with metal particles, and therefore their diffusion to the metal-support interface was favored, leaving the top surface of the metal particle for further adsorption of carbonaceous compounds [89]. Other authors reported the formation of filamentous coke in the ethanol steam reforming [27,28,56,90]. As detected by XRD analysis, TEM images also proved that growth of Ni particles took place, since large Ni agglomerates appeared. Sharma et al. [16] stated that the size of the metal particles plays a key role in coke location. An increase in the metal particle size promotes coke formation and favours the growth of especially filamentous coke.

The decay in the activity of 10 wt%NiO/CaO bifunctional catalyst may be attributed to the poor dispersion of Ni and the location of the coke. In fact, low amounts of coke together with poor Ni dispersion influence catalyst activity [89]. Several authors report Ni sintering as the main deactivation cause in sorption enhanced steam reforming processes [91–94].

4. Conclusions

A 10 wt%NiO/CaO bifunctional catalyst performed well in the sorption enhanced ethanol steam reforming in the 600–750 °C temperature range. At zero time on stream, an increase in temperature enhanced ethanol steam reforming reactions and increased H_2

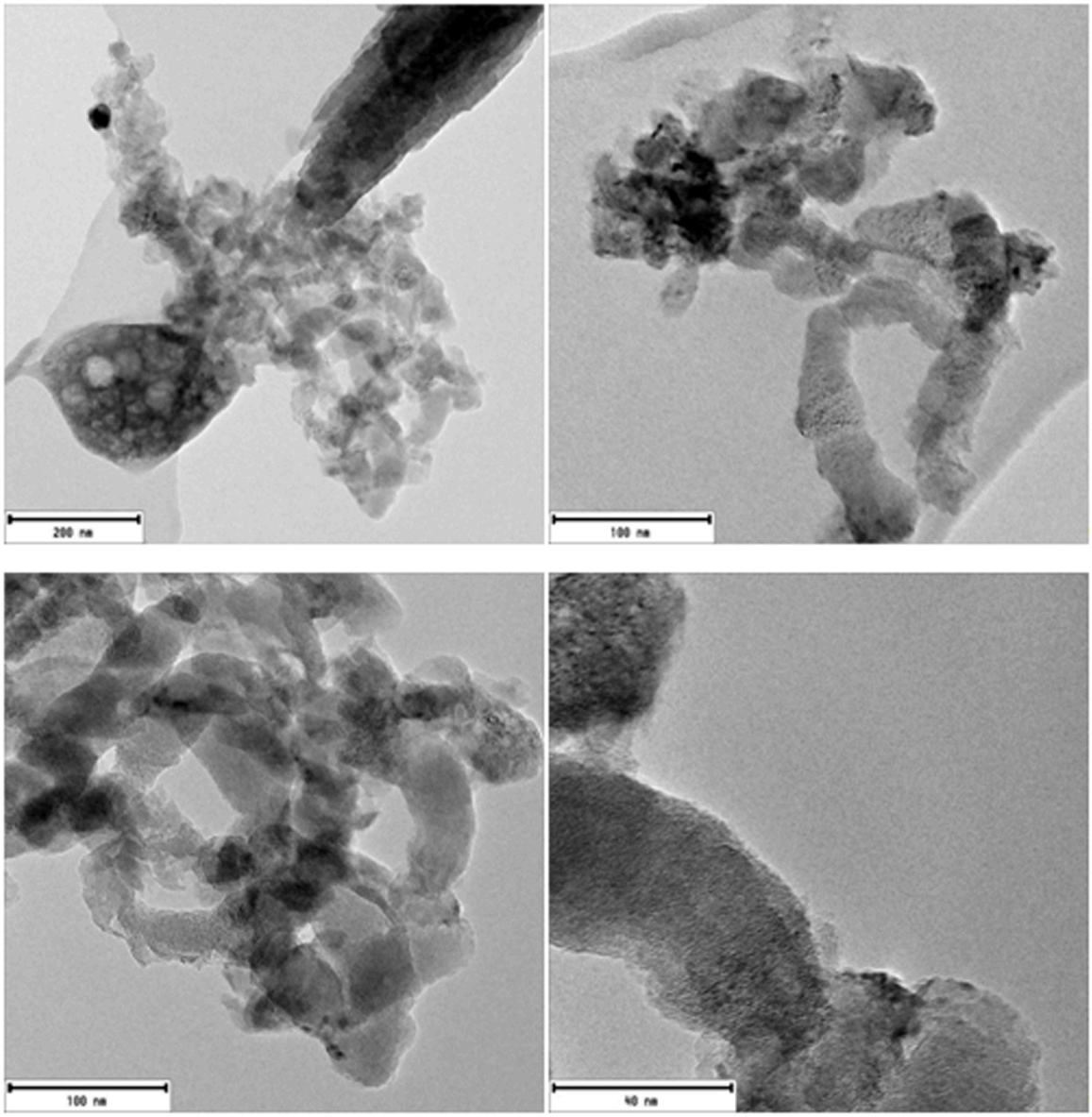

Fig. 8. TEM images of coke deposition on the deactivated Ni/CaO catalyst.

production, reaching a peak of 22.3 wt% at 700 °C. However, high temperatures hindered catalyst sorption performance, and so CO_2 sorption capacity, with the maximum CO_2 uptake being 7.9 $mmol_{CO2}$ g_{cat}^{-1} at 600 °C.

The stability of the catalyst was tested over 22 SEESR/desorption cycles. The adsorption capacity of the catalyst decreased from 6 to 5.6 $mmol_{CO2}$ g_{cat}^{-1} after 12 cycles, which meant a reduction of around 7%, and therefore a slight decrease in H_2 production from 22.24 wt% in the first cycle to 18.46 wt% in the 12th cycle. This value remained approximately constant in subsequent cycles. These results evidenced that desorption at the reforming temperature attenuated catalyst deactivation and improved its stability, since it allowed slowing down catalyst sorption decay.

Due to the CO_2 sorption capacity of CaO, its particles re-disperse during SEESR and subsequent desorption. These structural changes over multiple cycles were responsible for the moderate decrease in the sorption capacity of the support. As a result, Ni particles also relocated and tended to agglomerate and form larger Ni crystallites. Therefore, changes in the catalyst structure together with coke deposition lead to the loss of active sites, hindering the adsorption of ethanol and water.

CRediT authorship contribution statement

Maria Cortazar: Investigation, Methodology, Writing – original draft, Visualization, Writing – review & editing. **Shuzhuang Sun:** Investigation, Resources, Visualization, Writing – review & editing. **Chunfei Wu:** Conceptualization, Validation, Writing – review & editing, Visualization, Supervision. **Laura Santamaria:** Validation, Visualization, Conceptualization, Writing – review & editing. **Leire Olazar:** Investigation, Visualization, Writing – review & editing. **Enara Fernandez:** Visualization, Conceptualization, Writing – review & editing. **Maite Artetxe:** Conceptualization, Writing – review & editing, Visualization, Supervision, Project administration, Funding acquisition. **Gartzen Lopez:** Methodology, Conceptualization, Validation, Writing – review & editing, Visualization, Supervision, Project administration, Funding acquisition. **Martin Olazar:** Writing – review & editing, Visualization, Supervision, Project administration, Funding acquisition.

Declaration of Competing Interest

The authors declare that they have no known competing financial interests or personal relationships that could have appeared to influence the work reported in this paper.

Acknowledgments

This work was carried out with financial support from the Spain's Ministries of Science, Innovation and Universities (RTI2018–098283-J-I00(MCIU/AEI/FEDER, UE) and (RTI2018–101678-BI00 MCIU/AEI/FEDER, UE) and Science and Innovation (PID2019–107357RB-I00 (MCI/AEI/FEDER, UE), the Basque Government (IT1218–19 and KK-2020/00107). This project has received funding from the European Union's Horizon 2020 research and innovation programme under the Marie Sklodowska-Curie grant agreement No 823745. Maria Cortazar also thanks the Basque Government for her research training grant.

References

[1] R.C. Pietzcker, S. Osorio, R. Rodrigues, Tightening EU ETS targets in line with the European Green Deal: Impacts on the decarbonization of the EU power sector, Appl. Energy 293 (2021), 116914.
[2] J.B. Skjærseth, Towards a European green deal: the evolution of EU climate and energy policy mixes, Int. Envir. Agreem. Polit. Law Econ. 21 (2021) 25–41.
[3] M. Hafner, P.P. Raimondi, Priorities and challenges of the EU energy transition: from the European green package to the new green deal, Russ. J. Econ. 6 (2021) 374–389.
[4] G. Kakoulaki, I. Kougias, N. Taylor, F. Dolci, J. Moya, A. Jäger-Waldau, Green hydrogen in Europe – A regional assessment: substituting existing production with electrolysis powered by renewables, Energy Convers. Manag. 228 (2021), 113649.
[5] U.K. Zore, S.G. Yedire, N. Pandi, S. Manickam, S.H. Sonawane, A review on recent advances in hydrogen energy, fuel cell, biofuel and fuel refining via ultrasound process intensification, Ultrason. Sonochem. 73 (2021), 105536.
[6] A. Kovač, M. Paranos, D. Marciuš, Hydrogen in energy transition: a review, Int. J. Hydrog. Energy 46 (2021) 10016–10035.
[7] A. Arregi, M. Amutio, G. Lopez, J. Bilbao, M. Olazar, Evaluation of thermochemical routes for hydrogen production from biomass: a review, Energy Convers. Manag. 165 (2018) 696–719.
[8] S. Bepari, D. Kuila, Steam reforming of methanol, ethanol and glycerol over nickel-based catalysts-A review, Int. J. Hydrog. Energy 45 (2020) 18090–18113.
[9] S. Bac, S. Keskin, A.K. Avci, Recent advances in materials for high purity H2 production by ethanol and glycerol steam reforming, Int. J. Hydrog. Energy 45 (2020) 34888–34917.
[10] S. Nanda, R. Rana, Y. Zheng, J.A. Kozinski, A.K. Dalai, Insights on pathways for hydrogen generation from ethanol, Sustain. Energy Fuels 1 (2017) 1232–1245.
[11] M. Razavian, S. Fatemi, M. Malek mohammadi, A. Nouralishahi, Nickel supported ZIF-8.PEG modified catalyst: a designed active catalyst with high H_2 productivity in steam reforming of ethanol at moderate temperature, J. Environ. Chem. Eng. 9 (2021), 105531.
[12] J.L. Contreras, J. Salmones, J.A. Colín-Luna, L. Nuño, B. Quintana, I. Córdova, B. Zeifert, C. Tapia, G.A. Fuentes, Catalysts for H_2 production using the ethanol steam reforming (a review), Int. J. Hydrog. Energy 39 (2014) 18835–18853.
[13] D. Zanchet, J.B.O. Santos, S. Damyanova, J.M.R. Gallo, J.M.C. Bueno, Toward understanding metal-catalyzed ethanol reforming, ACS Catal. 5 (2015) 3841–3863.
[14] K.D.P.L. Kumar, B.N. Naidu, B. Sarkar, P. Mondal, K. Ghosh, V.V.D.N. Prasad, Enhanced CO_2 utilization via methane tri-reforming over Ru incorporated Co/MgO-Al_2O_3 catalyst: influence of La and Ce promoters, J. Environ. Chem. Eng. 9 (2021), 105949.
[15] S. Ogo, Y. Sekine, Recent progress in ethanol steam reforming using non-noble transition metal catalysts: a review, Fuel Process. Technol. 199 (2020), 106238.
[16] Y.C. Sharma, A. Kumar, R. Prasad, S.N. Upadhyay, Ethanol steam reforming for hydrogen production: latest and effective catalyst modification strategies to minimize carbonaceous deactivation, Renew. Sustain. Energy Rev. 74 (2017) 89–103.
[17] M. Ni, D.Y.C. Leung, M.K.H. Leung, A review on reforming bio-ethanol for hydrogen production, Int. J. Hydrog. Energy 32 (2007) 3238–3247.
[18] T.K. Phung, T.L.M. Pham, A.-T. Nguyen, K.B. Vu, H.N. Giang, T.- Nguyen, T. C. Huynh, H.D. Pham, Effect of supports and promoters on the performance of Ni-based catalysts in ethanol steam reforming, Chem. Eng. Technol. 43 (2020) 672–688.
[19] S. Chitsazan, S. Sepehri, G. Garbarino, M.M. Carnasciali, G. Busca, Steam reforming of biomass-derived organics: interactions of different mixture components on Ni/Al_2O_3 based catalysts, Appl. Catal., B. 187 (2016) 386–398.
[20] J. Comas, F. Marino, M. Laborde, N. Amadeo, Bio-ethanol steam reforming on Ni/Al_2O_3 catalyst, Chem. Eng. J. 98 (2004) 61–68.
[21] A.L. Alberton, M.M.V.M. Souza, M. Schmal, Carbon formation and its influence on ethanol steam reforming over Ni/Al_2O_3 catalysts, Catal. Today 123 (2007) 257–264.
[22] M.C. Sánchez-Sánchez, R.M. Navarro, J.L.G. Fierro, Ethanol steam reforming over Ni/La–Al_2O_3 catalysts: influence of lanthanum loading, Catal. Today 129 (2007) 336–345.
[23] A.J. Vizcaíno, P. Arena, G. Baronetti, A. Carrero, J.A. Calles, M.A. Laborde, N. Amadeo, Ethanol steam reforming on Ni/Al_2O_3 catalysts: effect of Mg addition, Int. J. Hydrog. Energy 33 (2008) 3489–3492.
[24] V. Claude, J.G. Mahy, S. Douven, T. Lohay, F. Micheli, S.D. Lambert, Sol-gel Ni-based/γ-Al_2O_3 as efficient catalysts for toluene reforming: catalytic activity during long-term experiments and in presence of H_2S, J. Environ. Chem. Eng. 8 (2020), 104528.
[25] Y. Wang, M.Z. Memon, M.A. Seelro, W. Fu, Y. Gao, Y. Dong, G. Ji, A review of CO_2 sorbents for promoting hydrogen production in the sorption-enhanced steam reforming process, Int. J. Hydrog. Energy (2021).
[26] H. Sun, Y. Wang, S. Xu, A.I. Osman, G. Stenning, J. Han, S. Sun, D. Rooney, P. T. Williams, F. Wang, C. Wu, Understanding the interaction between active sites and sorbents during the integrated carbon capture and utilization process, Fuel 286 (2021), 119308.
[27] J. Wang, D. Kang, B. Shen, H. Sun, C. Wu, Enhanced hydrogen production from catalytic biomass gasification with in-situ CO_2 capture, Environ. Pollut. 267 (2020), 115487.
[28] C. Quan, N. Gao, H. Wang, H. Sun, C. Wu, X. Wang, Z. Ma, Ethanol steam reforming on Ni/CaO catalysts for coproduction of hydrogen and carbon nanotubes, Int. J. Energy Res. 43 (2019) 1255–1271.
[29] H. Sun, J. Wang, J. Zhao, B. Shen, J. Shi, J. Huang, C. Wu, Dual functional catalytic materials of Ni over Ce-modified CaO sorbents for integrated CO_2 capture and conversion, Appl. Catal., B. 244 (2019) 63–75.
[30] M.M. Shahid, S.Z. Abbas, F. Maqbool, S. Ramirez-Solis, V. Dupont, T. Mahmud, Modeling of sorption enhanced steam methane reforming in an adiabatic packed bed reactor using various CO_2 sorbents, J. Environ. Chem. Eng. 9 (2021), 105863.
[31] A. Nawar, M. Ali, A.H. Khoja, A. Waqas, M. Anwar, M. Mahmood, Enhanced CO_2 capture using organic acid structure modified waste eggshell derived CaO sorbent, J. Environ. Chem. Eng. 9 (2021), 104871.
[32] C. Dang, J. Long, H. Li, W. Cai, H. Yu, Pd-promoted Ni-Ca-Al bi-functional catalyst for integrated sorption-enhanced steam reforming of glycerol and methane reforming of carbonate, Chem. Eng. Sci. 230 (2021), 116226.

[33] C. Dang, W. Yang, J. Zhou, W. Cai, Porous Ni-Ca-Al-O bi-functional catalyst derived from layered double hydroxide intercalated with citrate anion for sorption-enhanced steam reforming of glycerol, Appl. Catal., B. 298 (2021), 120547.

[34] G. Ji, J.G. Yao, P.T. Clough, J.C.D. Da Costa, E.J. Anthony, P.S. Fennell, W. Wang, M. Zhao, Enhanced hydrogen production from thermochemical processes, Energy Environ. Sci. 11 (2018) 2647–2672.

[35] N. Hanchate, S. Ramani, C.S. Mathpati, V.H. Dalvi, Biomass gasification using dual fluidized bed gasification systems: a review, J. Clean. Prod. 280 (2021).

[36] M.Z. Memon, X. Zhao, V.S. Sikarwar, A.K. Vuppaladadiyam, S.J. Milne, A. P. Brown, J. Li, M. Zhao, Alkali metal CO_2 sorbents and the resulting metal carbonates: potential for process intensification of sorption-enhanced steam reforming, Environ. Sci. Technol. 51 (2017) 12–27.

[37] C.K.S. Choong, Z. Zhong, L. Huang, Z. Wang, T.P. Ang, A. Borgna, J. Lin, L. Hong, L. Chen, Effect of calcium addition on catalytic ethanol steam reforming of Ni/Al_2O_3: I. Catalytic stability, electronic properties and coking mechanism, Appl. Catal., A. 407 (2011) 145–154.

[38] V. Nichele, M. Signoretto, F. Pinna, F. Menegazzo, I. Rossetti, G. Cruciani, G. Cerrato, A. Di, Michele, Ni/ZrO_2 catalysts in ethanol steam reforming: inhibition of coke formation by CaO-doping, Appl. Catal., B. 150- 151 (2014) 12–20.

[39] M. Shokrollahi Yancheshmeh, H.R. Radfarnia, M.C. Iliuta, High temperature CO_2 sorbents and their application for hydrogen production by sorption enhanced steam reforming process, Chem. Eng. J. 283 (2016) 420–444.

[40] N.H. Florin, A.T. Harris, Enhanced hydrogen production from biomass with in situ carbon dioxide capture using calcium oxide sorbents, Chem. Eng. Sci. 63 (2008) 287–316.

[41] H. Li, Y. Wang, N. Zhou, L. Dai, W. Deng, C. Liu, Y. Cheng, Y. Liu, K. Cobb, P. Chen, R. Ruan, Applications of calcium oxide–based catalysts in biomass pyrolysis/gasification – a review, J. Clean. Prod. 291 (2021), 125826.

[42] H. Sun, C. Wu, B. Shen, X. Zhang, Y. Zhang, J. Huang, Progress in the development and application of CaO-based adsorbents for CO_2 capture—a review, Mater. Today Sustainability 1-2 (2018) 1–27.

[43] S.A. Salaudeen, B. Acharya, A. Dutta, CaO-based CO_2 sorbents: a review on screening, enhancement, cyclic stability, regeneration and kinetics modelling, J. CO2 Util. 23 (2018) 179–199.

[44] A.N. Antzara, A. Arregi, E. Heracleous, A.A. Lemonidou, In-depth evaluation of a ZrO2 promoted CaO-based CO_2 sorbent in fluidized bed reactor tests, Chem. Eng. J. 333 (2018) 697–711.

[45] B. Dou, C. Wang, Y. Song, H. Chen, B. Jiang, M. Yang, Y. Xu, Solid sorbents for in-situ CO_2 removal during sorption-enhanced steam reforming process: a review, Renew. Sustain. Energy Rev. 53 (2016) 536–546.

[46] A.M. Kierzkowska, R. Pacciani, C.R. Müller, CaO-based CO_2 sorbents: from fundamentals to the development of new, highly effective materials, ChemSusChem 6 (2013) 1130–1148.

[47] A. Erkiaga, G. Lopez, I. Barbarias, M. Artetxe, M. Amutio, J. Bilbao, M. Olazar, HDPE pyrolysis-steam reforming in a tandem spouted bed-fixed bed reactor for H2 production, J. Anal. Appl. Pyrolysis 116 (2015) 34–41.

[48] A. Xu, W. Zhou, X. Zhang, B. Zhao, L. Chen, L. Sun, W. Ding, S. Yang, H. Guan, B. Bai, Gas production by catalytic pyrolysis of herb residues using Ni/CaO catalysts, J. Anal. Appl. Pyrolysis 130 (2018) 216–223.

[49] N. Chanburanasiri, A.M. Ribeiro, A.E. Rodrigues, A. Arpornwichanop, N. Laosiripojana, P. Praserthdam, S. Assabumrungrat, Hydrogen production via sorption enhanced steam methane reforming process using Ni/CaO multifunctional catalyst, Ind. Eng. Chem. Res. 50 (2011) 13662–13671.

[50] L. Liu, D. Hong, N. Wang, X. Guo, High purity H_2 production from sorption enhanced bio-ethanol reforming via sol-gel-derived Ni–CaO–Al_2O_3 bi-functional materials, Int. J. Hydrog. Energy 45 (2020) 34449–34460.

[51] S.B. Jo, J.H. Woo, J.H. Lee, T.Y. Kim, H.I. Kang, S.C. Lee, J.C. Kim, A novel integrated CO_2 capture and direct methanation process using Ni/CaO catal-sorbents, Sustain. Energy Fuels 4 (2020) 4679–4687.

[52] T. Nimmas, P. Jamrunroj, S. Wongsakulphasatch, W. Kiatkittipong, N. Laosiripojana, J. Gong, S. Assabumrungrat, Influence of CaO precursor on CO_2 capture performance and sorption-enhanced steam ethanol reforming, Int. J. Hydrog. Energy 44 (2019) 20649–20662.

[53] E.T. Santos, C. Alfonsín, A.J.S. Chambel, A. Fernandes, A.P. Soares Dias, C.I. C. Pinheiro, M.F. Ribeiro, Investigation of a stable synthetic sol–gel CaO sorbent for CO_2 capture, Fuel 94 (2012) 624–628.

[54] N. Gao, K. Chen, C. Quan, Development of CaO-based adsorbents loaded on charcoal for CO_2 capture at high temperature, Fuel 260 (2020), 116411.

[55] P. Teixeira, J. Hipólito, A. Fernandes, F. Ribeiro, C.I.C. Pinheiro, Tailoring synthetic Sol-Gel CaO sorbents with high reactivity or high stability for Ca-looping CO_2 capture, Ind. Eng. Chem. Res. 58 (2019) 8484–8494.

[56] S. Sang, Z. Zhao, H. Tian, Z. Sun, H. Li, S. Assabumrungrat, T. Muhammad, L. Zeng, J. Gong, Promotional role of MgO on sorption-enhanced steam reforming of ethanol over Ni/CaO catalysts, AIChE J. 66 (2020), e16877.

[57] L. He, H. Berntsen, De Chen, , Approaching sustainable H2 production: sorption enhanced steam reforming of ethanol, J. Phys. Chem. A. 114 (2010) 3834–3844.

[58] A. Lima da Silva, I.L. Müller, Hydrogen production by sorption enhanced steam reforming of oxygenated hydrocarbons (ethanol, glycerol, n-butanol and methanol): Thermodynamic modelling, Int. J. Hydrog. Energy 36 (2011) 2057–2075.

[59] C. Montero, A. Remiro, P.L. Benito, J. Bilbao, A.G. Gayubo, Optimum operating conditions in ethanol steam reforming over a Ni/La_2O_3-αAl_2O_3 catalyst in a fluidized bed reactor, Fuel Process. Technol. 169 (2018) 207–216.

[60] A.N. Antzaras, E. Heracleous, A.A. Lemonidou, Hybrid catalytic materials with CO_2 capture and oxygen transfer functionalities for high–purity H_2 production, Catal. Today 369 (2021) 2–11.

[61] C. Chen, C. Yu, W. Chen, Improvement of steam methane reforming via in-situ CO_2 sorption over a nickel-calcium composite catalyst, Int. J. Hydrog. Energy 46 (2021) 16655–16666.

[62] M. Hosseini Abbandanak, M. Taghizadeh, N. Fallah, High-purity hydrogen production by sorption-enhanced methanol steam reforming over a combination of Cu–Zn–CeO_2–ZrO_2/MCM-41 catalyst and (Li–Na–K) NO_3·MgO adsorbent, Int. J. Hydrog. Energy 46 (2021) 7099–7112.

[63] B. Valle, N. García-Gómez, A. Remiro, J. Bilbao, A.G. Gayubo, Dual catalyst-sorbent role of dolomite in the steam reforming of raw bio-oil for producing H_2-rich syngas, Fuel Process. Technol. 200 (2020), 106316.

[64] P. Pecharaumporn, S. Wongsakulphasatch, T. Glinrun, A. Maneedaeng, Z. Hassan, S. Assabumrungrat, Synthetic CaO-based sorbent for high-temperature CO_2 capture in sorption-enhanced hydrogen production, Int. J. Hydrog. Energy 44 (2019) 20663–20677.

[65] Z.- Li, N.- Cai, Modeling of multiple cycles for sorption-enhanced steam methane reforming and sorbent regeneration in fixed bed reactor, Energy Fuels 21 (2007) 2909–2918.

[66] A. Di Michele, A. Dell'Angelo, A. Tripodi, E. Bahadori, F. Sànchez, D. Motta, N. Dimitratos, I. Rossetti, G. Ramis, Steam reforming of ethanol over Ni/$MgAl_2O_4$ catalysts, Int. J. Hydrog. Energy 44 (2019) 952–964.

[67] A.C.V. Olivares, M.F. Gomez, M.N. Barroso, M.C. Abello, Ni-supported catalysts for ethanol steam reforming: effect of the solvent and metallic precursor in catalyst preparation, Int. J. Ind. Chem. 9 (2018) 61–73.

[68] J. Bussi, M. Musso, A. Quevedo, R. Faccio, M. Romero, Structural and catalytic stability assessment of Ni-La-Sn ternary mixed oxides for hydrogen production by steam reforming of ethanol, Catal. Today 296 (2017) 154–162.

[69] J. Shao, G. Zeng, Y. Li, Effect of Zn substitution to a $LaNiO_{3-\delta}$ perovskite structured catalyst in ethanol steam reforming, Int. J. Hydrog. Energy 42 (2017) 17362–17375.

[70] A. Di Giuliano, J. Girr, R. Massacesi, K. Gallucci, C. Courson, Sorption enhanced steam methane reforming by Ni–CaO materials supported on mayenite, Int. J. Hydrog. Energy 42 (2017) 13661–13680.

[71] I. Aloisi, A. Di Giuliano, A. Di Carlo, P.U. Foscolo, C. Courson, K. Gallucci, Sorption enhanced catalytic Steam Methane Reforming: experimental data and simulations describing the behaviour of bi-functional particles, Chem. Eng. J. 314 (2017) 570–582.

[72] P. Xu, Z.M. Zhou, C. Zhao, Z. Cheng, Ni/CaO-Al_2O_3 bifunctional catalysts for sorption-enhanced steam methane reforming, AIChE J. 60 (2014) 3547–3556.

[73] D. Li, H. Xue, R. Hu, Effect of Ce/Ca Ratio in Ni/CeO_2-ZrO_2-CaO catalysts on high-purity hydrogen production by sorption-enhanced steam reforming of acetic acid and bio-oil, Ind. Eng. Chem. Res. 59 (2020) 1446–1456.

[74] K.O. Christensen, D. Chen, R. Lødeng, A. Holmen, Effect of supports and Ni crystal size on carbon formation and sintering during steam methane reforming, Appl. Catal., A. 314 (2006) 9–22.

[75] L. Santamaria, G. Lopez, A. Arregi, M. Artetxe, M. Amutio, J. Bilbao, M. Olazar, Catalytic steam reforming of biomass fast pyrolysis volatiles over Ni–Co bimetallic catalysts, J. Ind. Eng. Chem. 91 (2020) 167–181.

[76] M. Artetxe, J. Alvarez, M.A. Nahil, M. Olazar, P.T. Williams, Steam reforming of different biomass tar model compounds over Ni/Al_2O_3 catalysts, Energy Convers. Manag. 136 (2017) 119–126.

[77] M. Artetxe, M.A. Nahil, M. Olazar, P.T. Williams, Steam reforming of phenol as biomass tar model compound over Ni/Al2O3 catalyst, Fuel 184 (2016) 629–636.

[78] A. Ochoa, I. Barbarias, M. Artetxe, A.G. Gayubo, M. Olazar, J. Bilbao, P. Castaño, Deactivation dynamics of a Ni supported catalyst during the steam reforming of volatiles from waste polyethylene pyrolysis, Appl. Catal., B. 209 (2017) 554–565.

[79] I. Barbarias, G. Lopez, M. Amutio, M. Artetxe, J. Alvarez, A. Arregi, J. Bilbao, M. Olazar, Steam reforming of plastic pyrolysis model hydrocarbons and catalyst deactivation, Appl. Catal., A. 527 (2016) 152–160.

[80] J. Vicente, J. Ereña, C. Montero, M.J. Azkoiti, J. Bilbao, A.G. Gayubo, Reaction pathway for ethanol steam reforming on a Ni/SiO_2 catalyst including coke formation, Int. J. Hydrog. Energy 39 (2014) 18820–18834.

[81] E. Fernandez, M. Amutio, M. Artetxe, A. Arregi, L. Santamaria, G. Lopez, J. Bilbao, M. Olazar, Assessment of product yields and catalyst deactivation in fixed and fluidized bed reactors in the steam reforming of biomass pyrolysis volatiles, Process Saf. Environ. Prot. 145 (2021) 52–62.

[82] A. Ochoa, A. Arregi, M. Amutio, A.G. Gayubo, M. Olazar, J. Bilbao, P. Castaño, Coking and sintering progress of a Ni supported catalyst in the steam reforming of biomass pyrolysis volatiles, Appl. Catal., B. 233 (2018) 289–300.

[83] L. Santamaria, A. Arregi, G. Lopez, M. Artetxe, M. Amutio, J. Bilbao, M. Olazar, Effect of La_2O_3 promotion on a Ni/Al_2O_3 catalyst for H_2 production in the in-line biomass pyrolysis-reforming, Fuel 262 (2020), 116593.

[84] A. Arregi, G. Lopez, M. Amutio, I. Barbarias, L. Santamaria, J. Bilbao, M. Olazar, Regenerability of a Ni catalyst in the catalytic steam reforming of biomass pyrolysis volatiles, J. Ind. Eng. Chem. 68 (2018) 69–78.

[85] A. Remiro, B. Valle, A.T. Aguayo, J. Bilbao, A.G. Gayubo, Operating conditions for attenuating Ni/La_2O_3–αAl_2O_3 catalyst deactivation in the steam reforming of bio-oil aqueous fraction, Fuel Process. Technol. 115 (2013) 222–232.

[86] D.Y. Aceves Olivas, M.R. Baray Guerrero, M.A. Escobedo Bretado, M. Marques da Silva Paula, J. Salinas Gutiérrez, V. Guzmán Velderrain, A. López Ortiz, V. Collins-Martínez, Enhanced ethanol steam reforming by CO_2 absorption using CaO, CaO*MgO or Na_2ZrO_3, Int. J. Hydrog. Energy 39 (2014) 16595–16607.

[87] C. Montero, A. Remiro, B. Valle, L. Oar-Arteta, J. Bilbao, A.G. Gayubo, Origin and nature of coke in ethanol steam reforming and its role in deactivation of Ni/La_2O_3–αAl_2O_3 catalyst, Ind. Eng. Chem. Res. 58 (2019) 14736–14751.

[88] S.A. Ghungrud, P.D. Vaidya, Improved hydrogen production from sorption-enhanced steam reforming of ethanol (SESRE) using multifunctional materials of

cobalt catalyst and Mg-, Ce-, and Zr-modified CaO sorbents, Ind. Eng. Chem. Res. 59 (2020) 693–703.
[89] A. Ochoa, J. Bilbao, A.G. Gayubo, P. Castaño, Coke formation and deactivation during catalytic reforming of biomass and waste pyrolysis products: a review, Renew. Sustain. Energy Rev. 119 (2020), 109600.
[90] J. Vicente, C. Montero, J. Ereña, M.J. Azkoiti, J. Bilbao, A.G. Gayubo, Coke deactivation of Ni and Co catalysts in ethanol steam reforming at mild temperatures in a fluidized bed reactor, Int. J. Hydrog. Energy 39 (2014) 12586–12596.
[91] S.M. Kim, P.M. Abdala, D. Hosseini, A. Armutlulu, T. Margossian, C. Copéret, C. Müller, Bi-functional Ru/$Ca_3Al_2O_6$-CaO catalyst-CO_2 sorbent for the production of high purity hydrogen: Via sorption-enhanced steam methane reforming, Catal. Sci. Technol. 9 (2019) 5745–5756.
[92] H. Li, S. Wu, C. Dang, G. Yang, Y. Cao, H. Wang, F. Peng, H. Yu, Production of high-purity hydrogen from paper recycling black liquor via sorption enhanced steam reforming, Green, Energy Environ. (2020).
[93] H. Li, H. Tian, S. Chen, Z. Sun, T. Liu, R. Liu, S. Assabumrungrat, J. Saupsor, R. Mu, C. Pei, J. Gong, Sorption enhanced steam reforming of methanol for high-purity hydrogen production over Cu-MgO/Al_2O_3 bifunctional catalysts, Appl. Catal., B. 276 (2020), 119052.
[94] X. Wang, Y. He, T. Xu, B. Xiao, S. Liu, Z. Hu, J. Li, CO_2 sorption-enhanced steam reforming of phenol using Ni–M/CaO–$Ca_{12}Al_{14}O_{33}$ (M =Cu, Co, and Ce) as catalytic sorbents, Chem. Eng. J. 393 (2020), 124769.